Electronic Supplementary Material (ESI) for Journal of Materials Chemistry C.

Interfacial design of gold/silver core-shell nanostars for plasmon enhanced photocatalytic coupling of 4-aminothiophenol

Gagandeep Kaur[1], Swati Tanwar[1], Vishaldeep Kaur[1], Rathindranath Biswas[2], Sangeeta Saini[3], Krishna Kanta Haldar[2]* and Tapasi Sen[1]*

[1]Institute of Nano Science and Technology, Mohali, 160062, India. E-mail: tapasi@inst.ac.in

[2]Department of Chemistry, Central University of Punjab, Bathinda, 151001, India. E-mail: krishnakanta.haldar@gmail.com

[3]Department of Chemistry, Kurukshetra University, Kurukshetra, 136119, India.

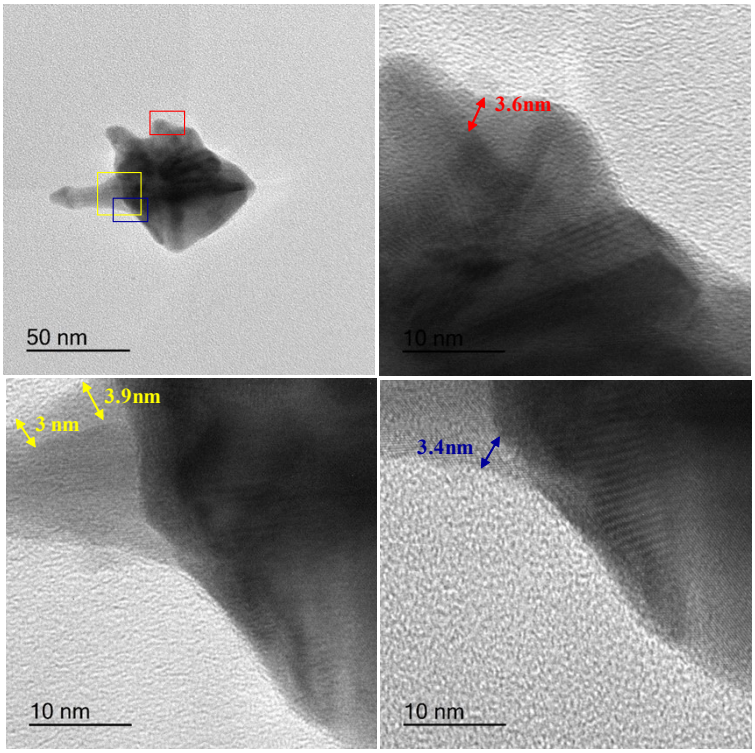

Figure. S1 High resolution TEM images of Au@Ag NS showing the thickness of Ag over the preformed Au NSs.

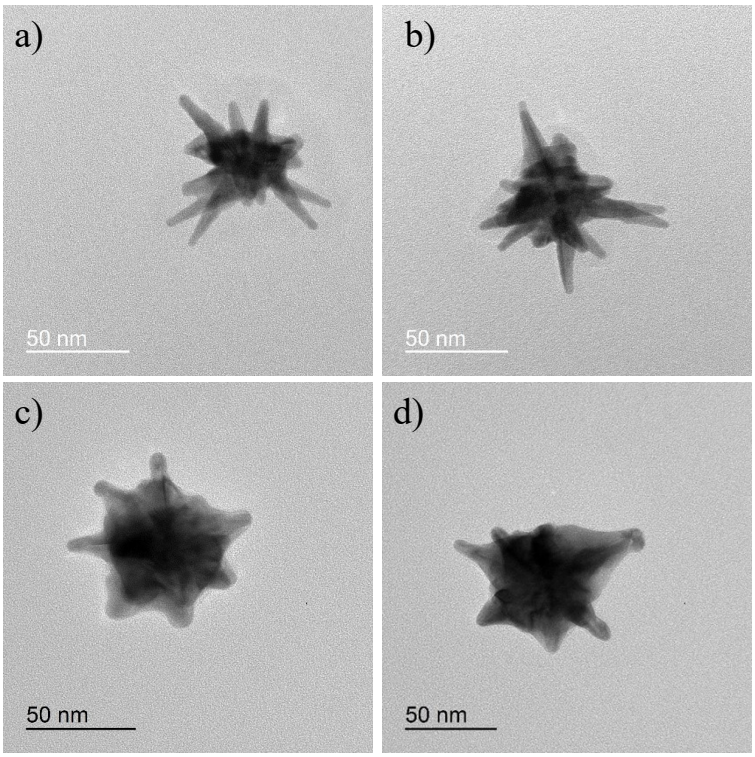

Figure. S2 TEM images of (a, b) Au NSs and (c, d) Au@Ag NSs.

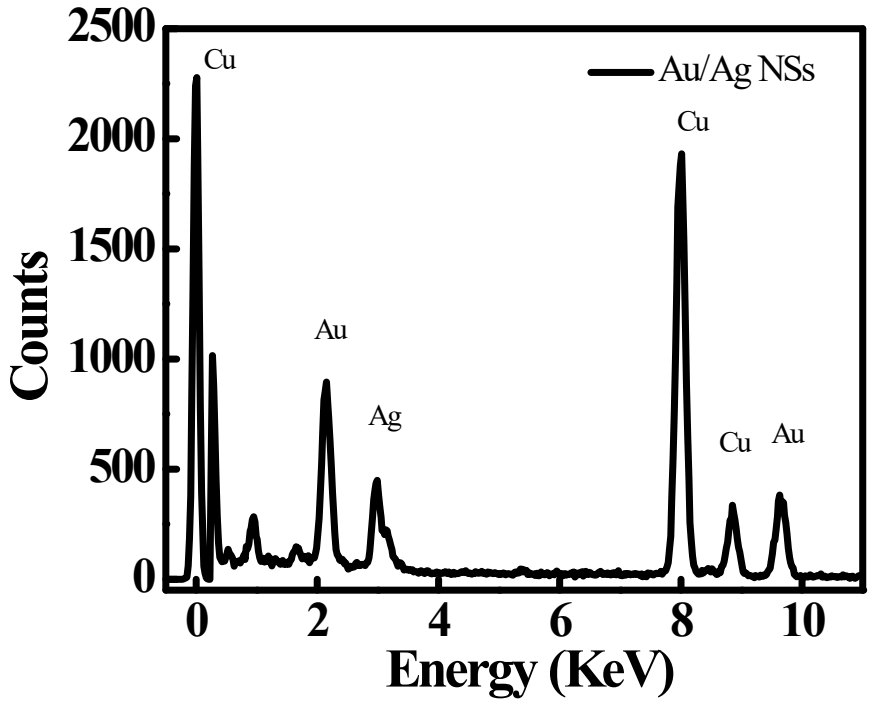

Figure. S3 TEM-EDX (Energy dispersive X-ray) spectrum of Au@Ag NSs.

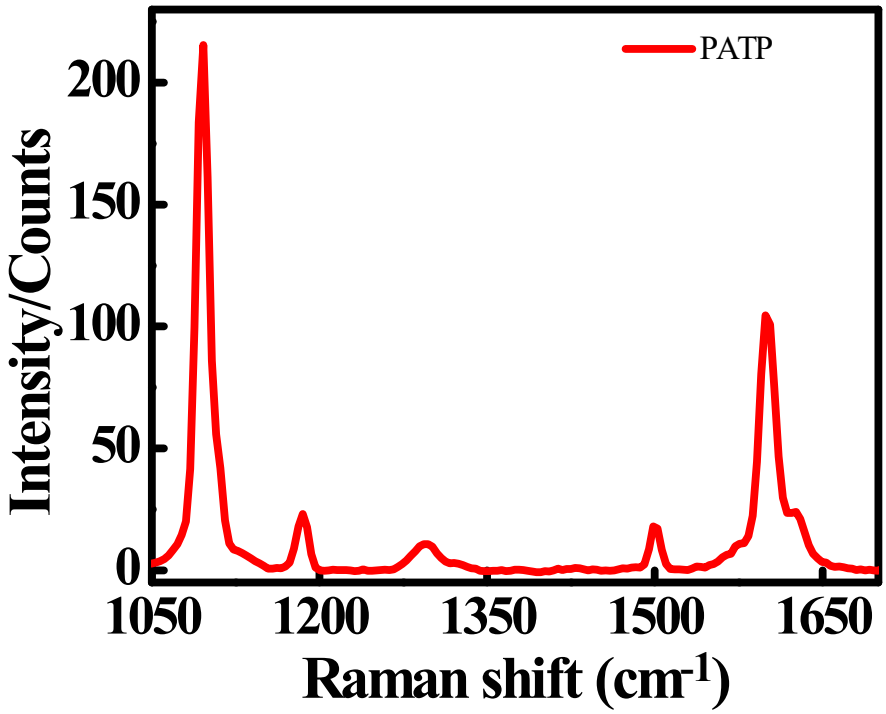

Figure. S4 Normal Raman spectrum of solid PATP.

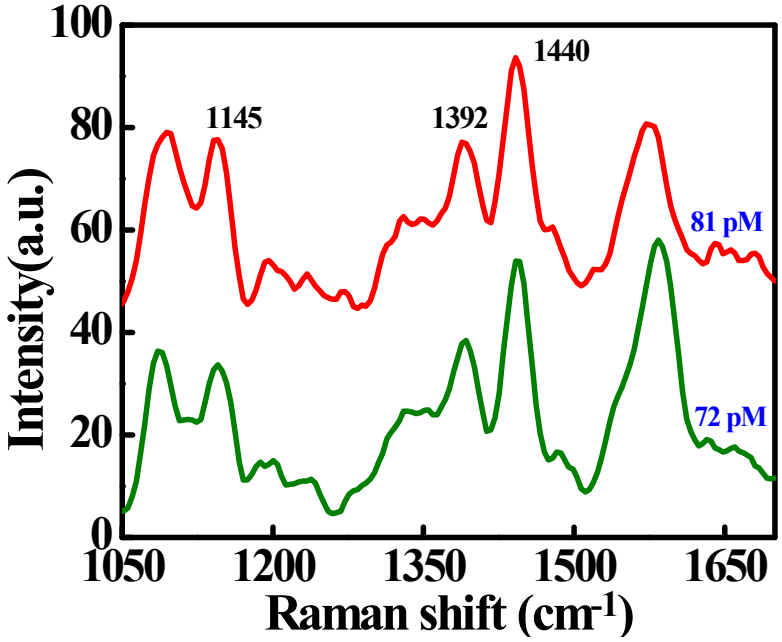

Figure. S5 Concentration dependent SERS spectra of DMAB formed from PATP at different concentrations of Au/Ag nanostars under acidic conditions.

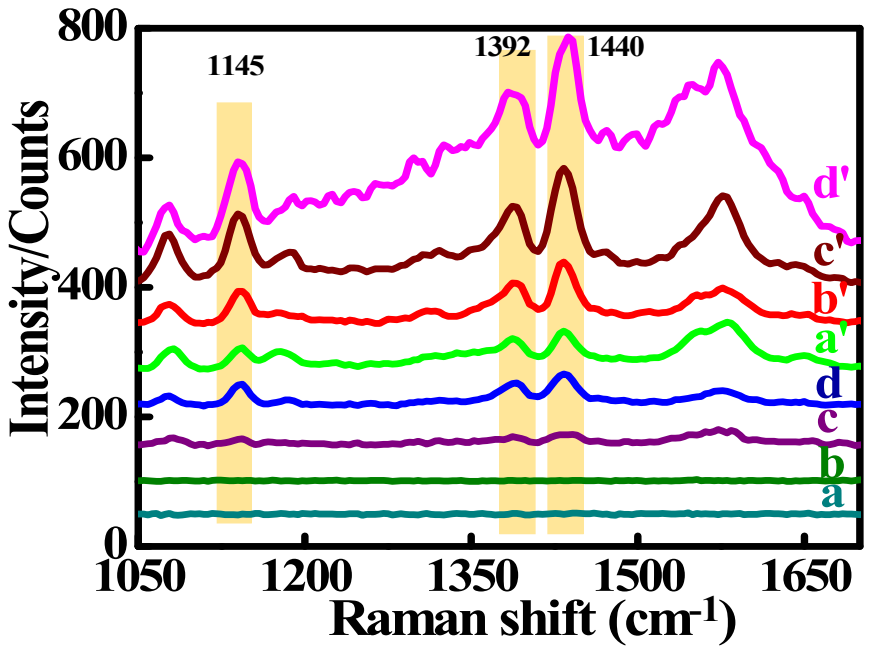

Figure. S6 SERS spectra of DMAB formed from PATP at incubation time of 512s using 45 pM concentration of Au NS (a), and Au/Ag NSs (a'); 63 pM concentration of Au NS (b), and Au/Ag NSs (b'); 81 pM concentration of Au NS (c), and Au/Ag NSs (c'); and 180 pM concentration of Au NS (d), and Au/Ag NSs (d').

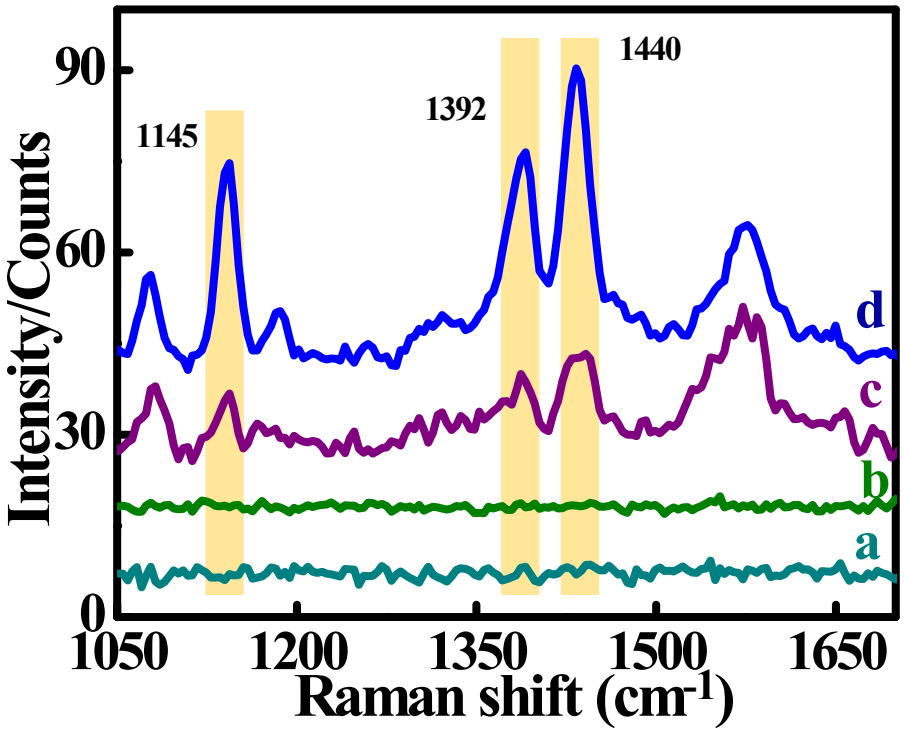

Figure. S7 Magnified SERS spectra of DMAB formed from PATP at incubation time of 512s using 45 pM concentration of Au NS (a), 63 pM concentration of Au NS (b), 81 pM concentration of Au NS (c), and 180 pM concentration of Au NS (d).

FDTD (finite difference time domain) simulation.

The electric field magnitude, |E| is computed through three-dimensional finite-difference time-domain (FDTD) modelling for Au nanostar as well as for Ag coated Au nanostar using commercial-grade simulator Lumerical Software (https://www.lumerical.com/products/-fdtd/). The plots in Figure S8 indicate increase in |E| at tips for Ag coated Au nanostar as compared to uncoated pure Au nanostar. The enhancement in electric field as obtained from Au core/Ag shell NS compared to pure Au NS will result in higher SERS enhancement of DMAB formed from PATP for Au core/Ag shell nanostar than that of Au nanostar which are in good agreement with experimental findings.

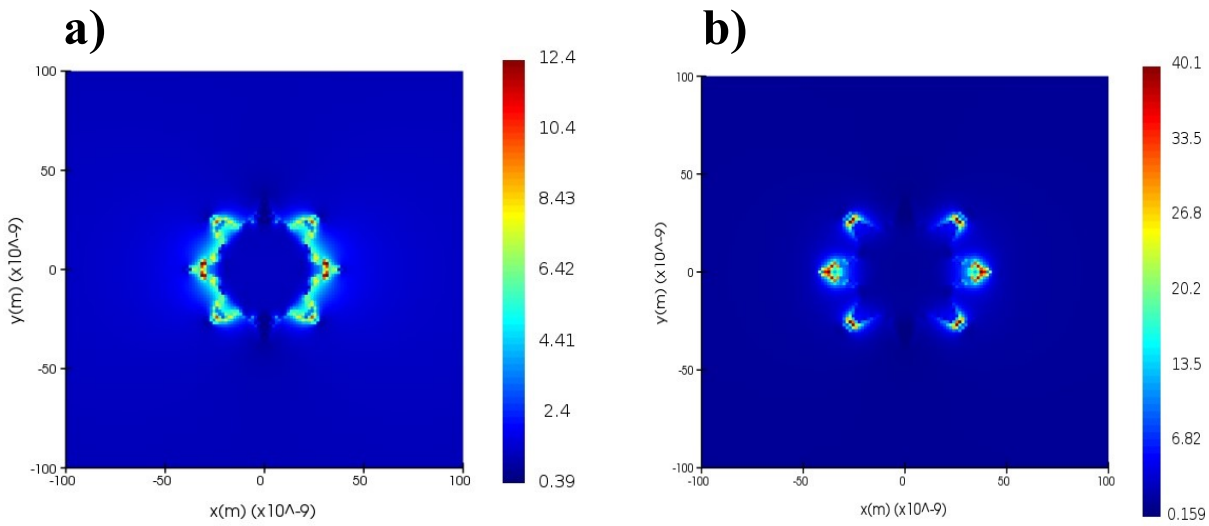

Figure. S8 The magnitude of electric field |E| in xy plane passing through the centre of nanostar at λ=540 nm for (a) Au-nanostar (b) silver coated Au-nanostar. A plane wave source has been used for FDTD calculations. The incident wave-vector is perpendicular to plotted xy cross-section. Note the difference in color-coding scale for both the plots.

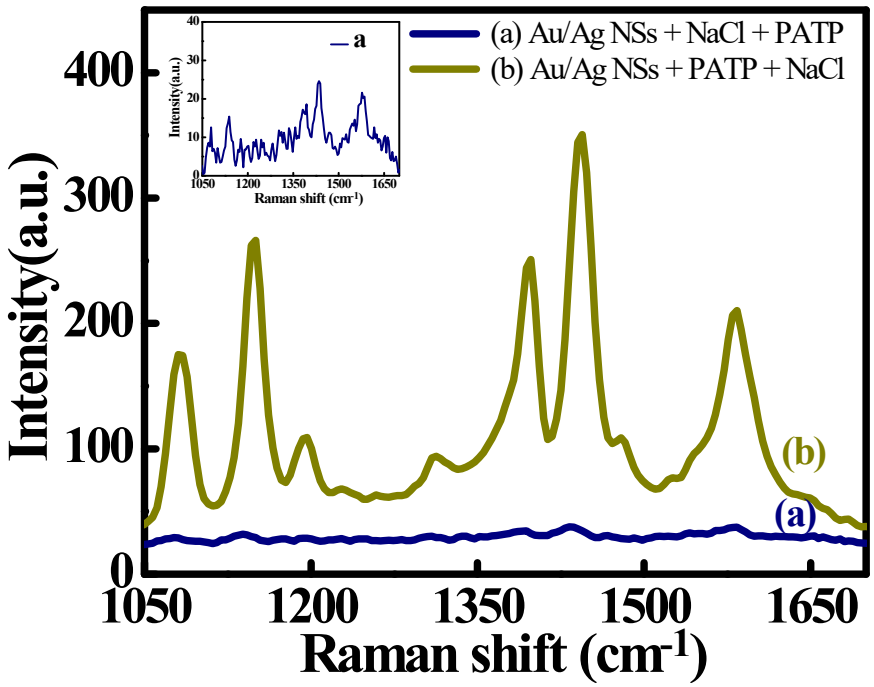

Figure. S9 SERS spectra of DMAB formed from PATP at 180pM concentration of Au/Ag NSs at a) zero second incubation time and b) 512 seconds incubation time.

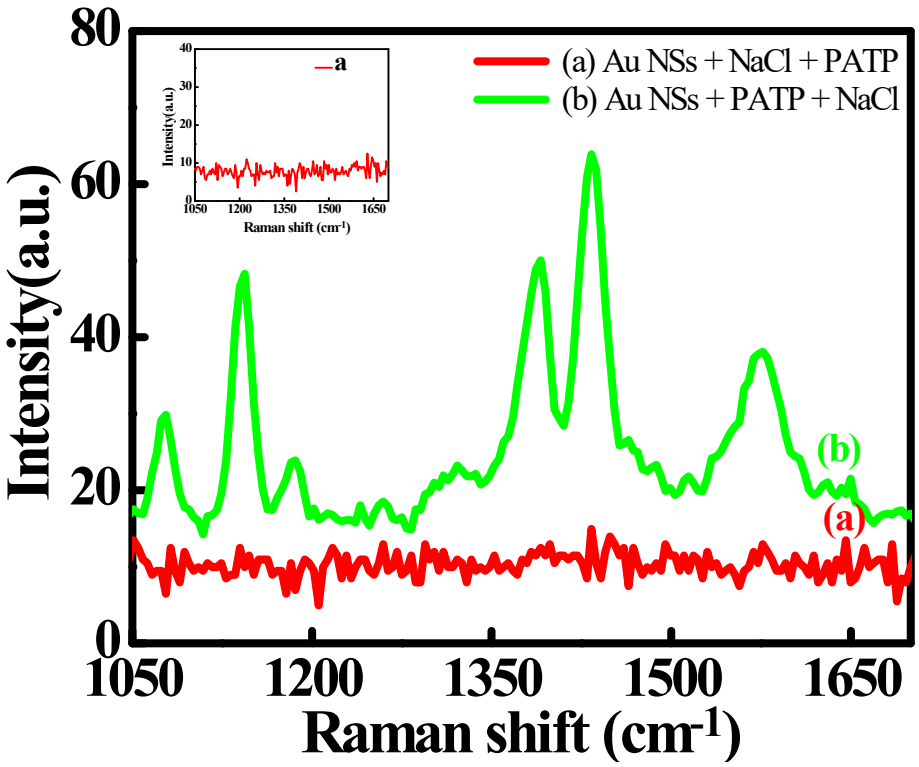

Figure. S10 SERS spectra of DMAB formed from PATP at 180pM concentration of Au NSs at a) zero second incubation time and b) 512 seconds incubation time.

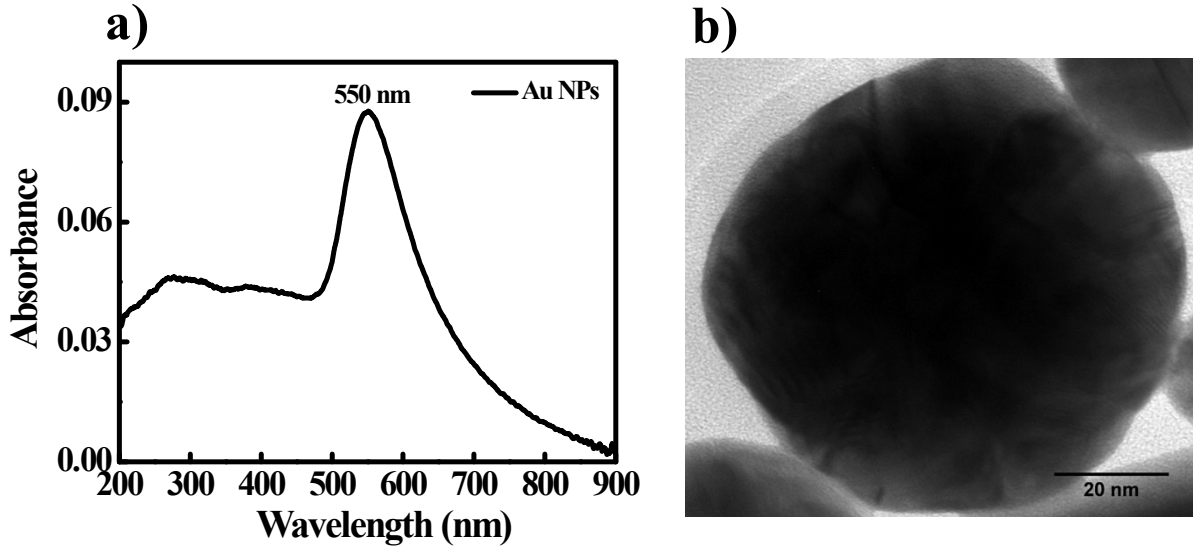

Figure. S11 a) UV-Vis absorption spectrum b) TEM image of as prepared spherical Au nanoparticles.

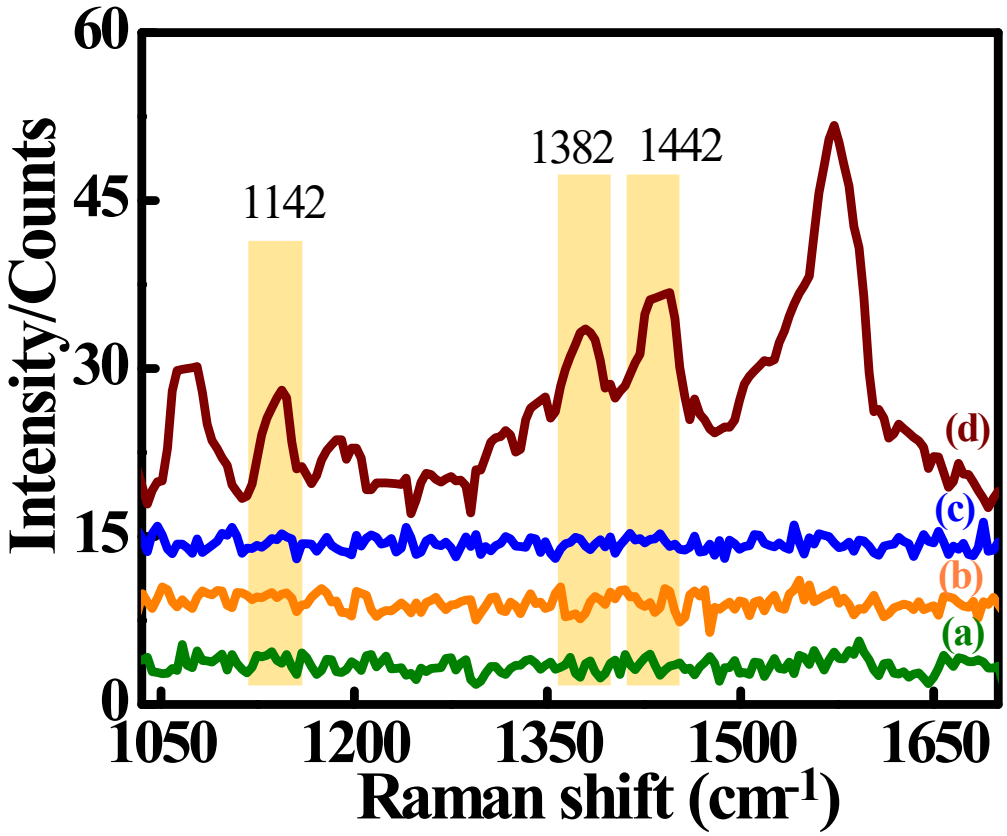

Figure. S12 SERS spectra of DMAB formed from PATP using spherical Au NPs at 45 pM (a), 63 pM (b), 81 pM (c), 180 pM (d) concentration at incubation time 512s.

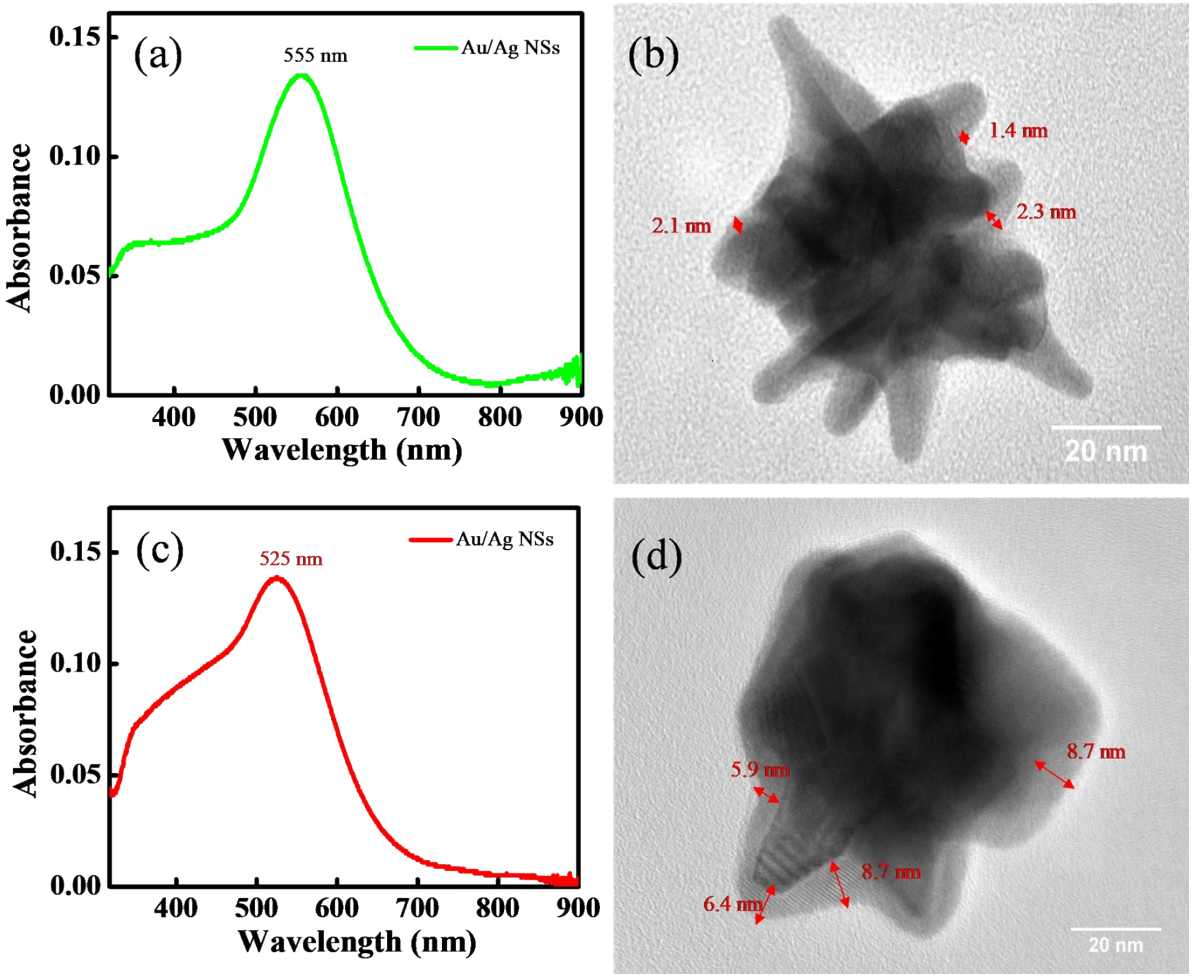

Figure. S13 UV-Vis absorption spectra and TEM images of Au/Ag NSs with lower Ag coating (a,b) and with higher Ag coating (c,d).

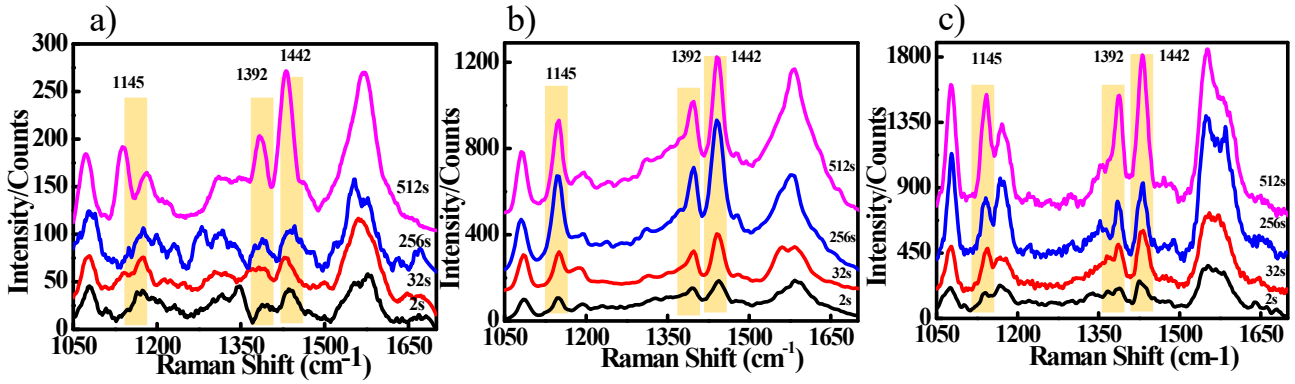

Figure. S14 Time dependent SERS spectra of DMAB formed from PATP at 36 pM concentration of Au/Ag NSs with a) lower Ag coating (1.9 ± 0.5 nm), b) moderate Ag coating (3.5 ± 0.5 nm), and c) higher Ag coating (7 ± 0.5 nm).

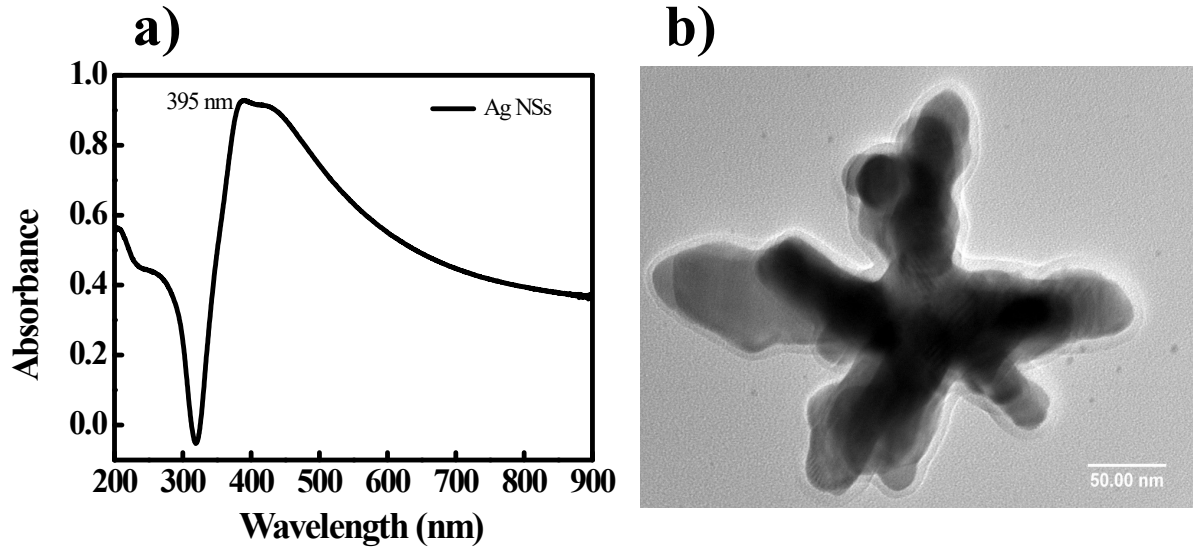

Figure. S15 a) UV-Vis absorption spectrum, and b) TEM image of as prepared Ag NSs.

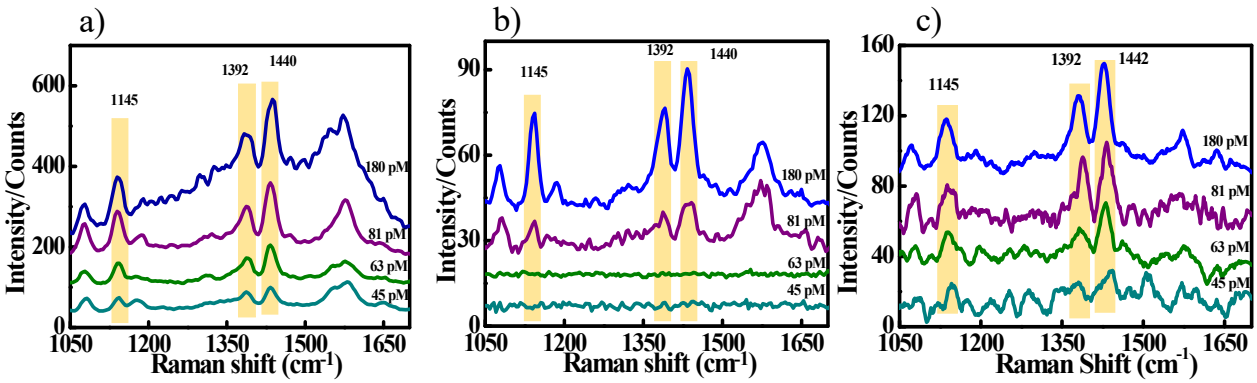

Figure. S16 SERS spectra of DMAB formed from PATP at incubation time of 512s using different concentrations of a) Au/Ag NSs, b) Au NSs, and c) Ag NSs.

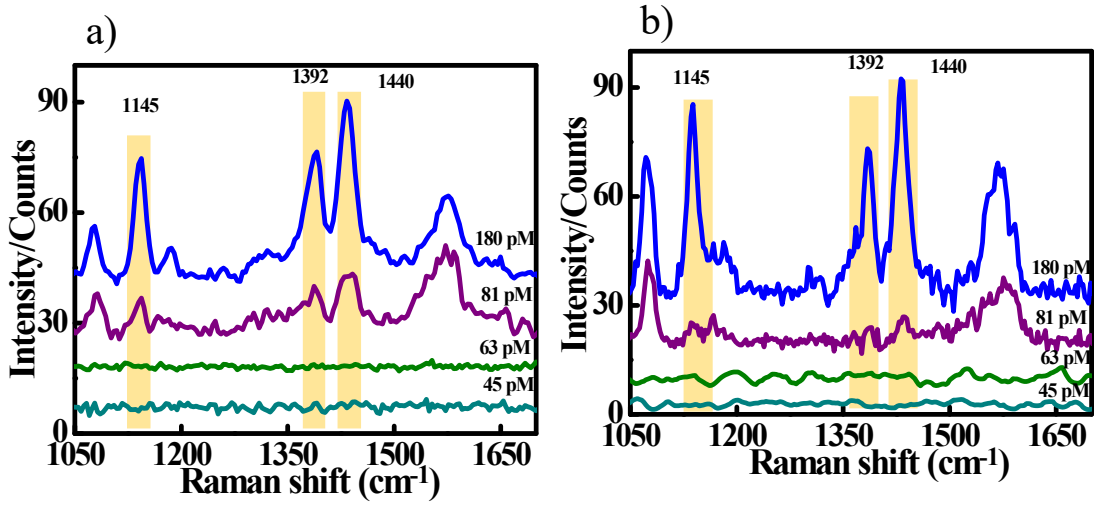

Figure. S17 SERS spectra of DMAB formed from PATP at incubation time of 512s using different concentrations of Au NSs at a) 532 nm laser, and b) 633 nm laser.

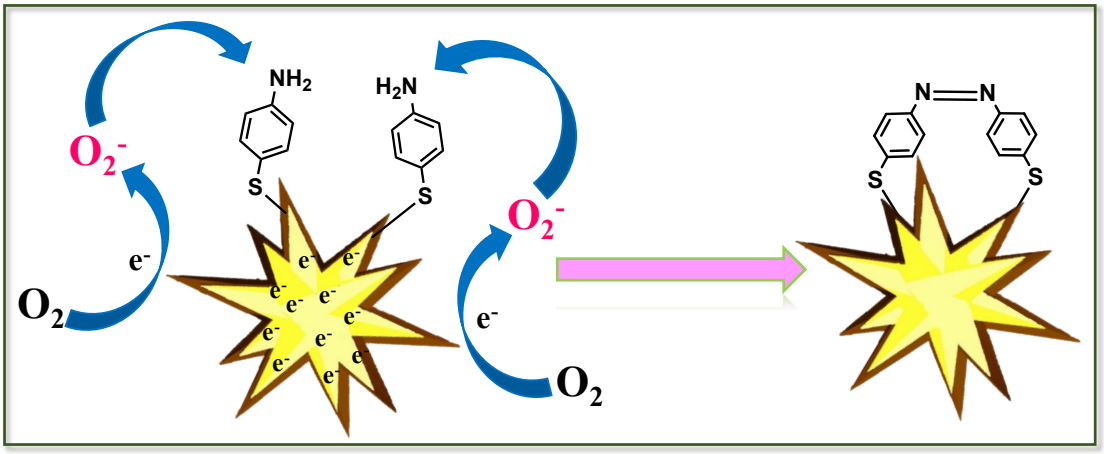

Figure. S18 Schematic illustration for the reaction mechanism depicting the oxidation of PATP into DMAB.

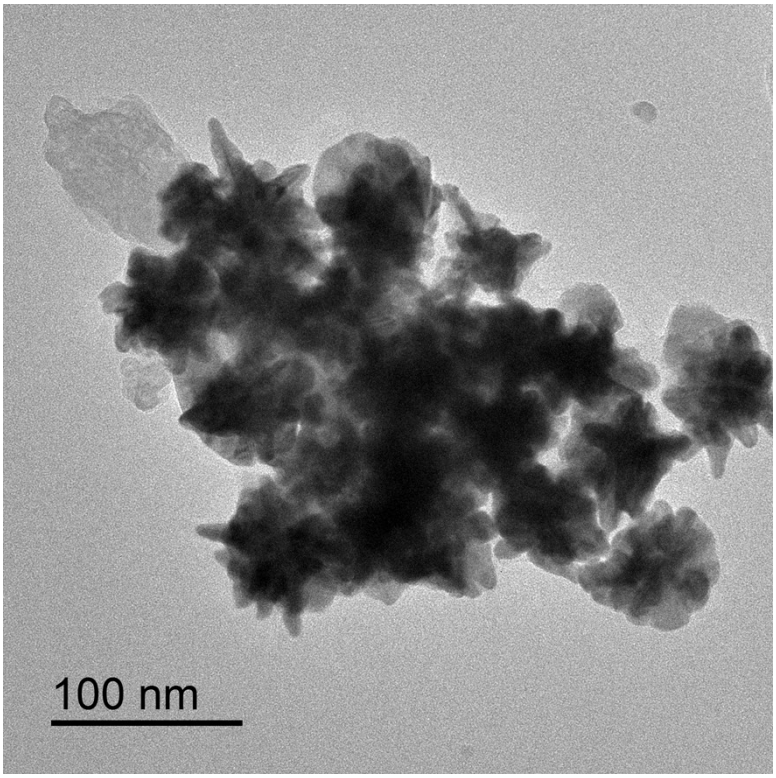

Figure. S19 TEM images of Au/Ag NSs after catalytic reaction of PATP to DMAB.

Concentration calculation of Au NSs.

For the determination of concentration of Au/Ag nanostars, we had exploited beer- lambert's law as described in equation (1).

$$\text{Absorbance (A)} = \varepsilon cl \qquad (1)$$

Where Ɛ is extinction coefficient of Au NSs (20.1×10^8 M^{-1} cm^{-1} for LSPR-710 nm)[1], c is concentration and l is path length (1 cm).

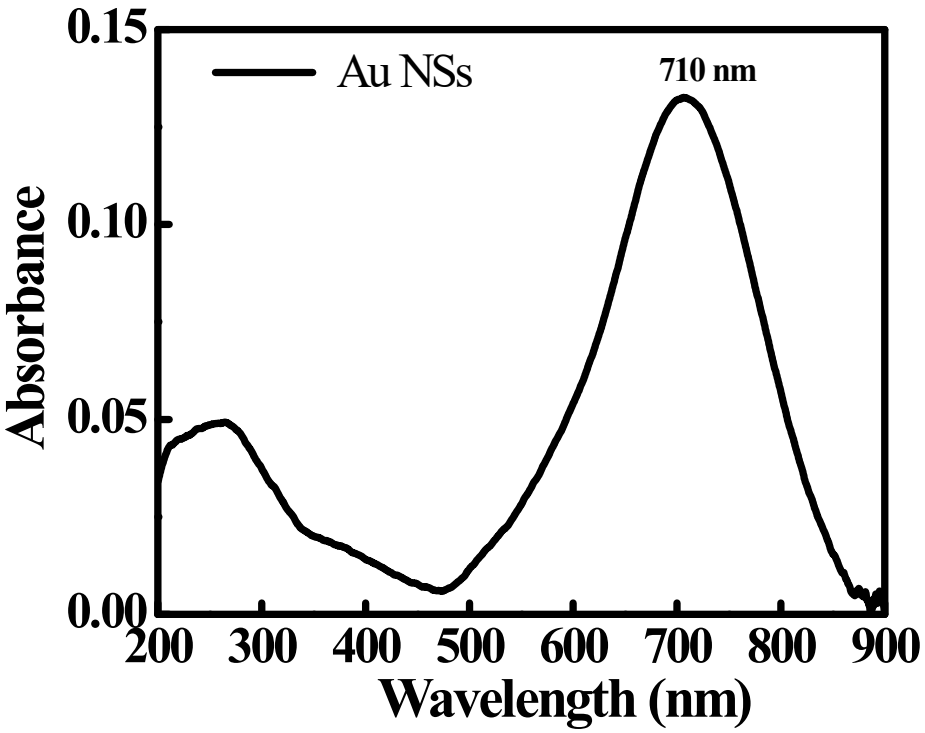

Figure. S20 UV-Vis absorption spectrum of Au nanostars after washing the reaction mixture.

The concentration of Au NSs was found to be 13373 pM by using the equation (1)

The total concentrations of Au NSs (Au/Ag NSs) used for the photocatalytic conversions of PATP into DMAB were 180, 81, 72, 63, 54, 45, 36, 27, 18, 9 pM in total reaction volume of 820 µl.

Now, we have assumed that all the Au nanostars are coated with Ag shell so the concentration of the Au/Ag nanostars is same as the Au nanostars.

Concentration calculation of Ag NSs.

The concentration of Ag NSs was calculated according to the method given by K. Kalishwaralal et al.[2] The concentration of Ag NSs was found to be 0.4 nM which is consistent with the report published by Oliveira et al.[3] Different concentrations of Ag NSs were attained through centrifugation at 2500 rcf for 10 minutes with temperature of 4˚C. The SERS spectra of DMAB formed from PATP were recorded using Ag NSs at different concentrations such as 180, 81, 63, 45 pM in total reaction mixture of 820 µl.

Details of SERS spectra measurement in inert atmosphere.

For the dimerization reaction of PATP into DMAB, whether atmospheric oxygen is required or not, we had performed the control reaction in absence of oxygen i.e. in inert atmosphere. For this, two neck round bottom flask was attached with a balloon filled with nitrogen gas attached with one neck of r.b.f. The r.b.f was filled with nitrogen gas and other neck was covered with septum. After that, with help of needle attached with syringe, PATP solution and Au/Ag nanostars solution were added through neck covered with septum. After different time intervals, the solution was precipitated with NaCl solution which is generally used for creating aggregated nanostructures. Upon addition of NaCl, solid aggregates were formed and collected through centrifugation and these aggregates were used for SERS measurement.

Table S1 ICP-MS (Inductively coupled plasma mass spectrometry) of Au/Ag nanostars.

Au and Ag concentrations are determined from ICP-MS and their atomic ratio is calculated by dividing the Au and Ag concentration with molar mass of Au (196.97 g mol^{-1}) and Ag (107.87g mol^{-1})

Nanoparticles	**Au conc. (mg/l)**	**Ag conc. (mg/l)**	**Atomic percentage**
Au/Ag NSs	0.42	0.22	Au: 51.1% and Ag: 48.9%

Table S2 The atomic percentage of Au and Ag in Au/Ag NSs from TEM- Energy dispersive X-ray (EDX) analysis is shown below.

Nanoparticles	**Atomic percentage (%) of Au and Ag**	
Au/Ag NSs (lower coating)	Au: 70.84%	Ag: 29.14%
Au/Ag NSs (higher coating)	Au: 41.15%	Ag: 58.85%

Table S3 ATR-FTIR frequency data (cm^{-1}) of PATP and DMAB.

Assignments	**PATP** ATR-FTIR frequency (cm^{-1})	**DMAB** ATR-FTIR frequency (cm^{-1})	**References**
*v*N-H	3418, 3320, 3206	3404, 3318	[4, 5]
νC-H	3021 2982	2976 2828	[6]
*v*S-H	2597 2560	Not ditected	[4, 7]
*v*C=C	1587 1488	1653 1491	[8]
*v*N=N	-	1444 1389	[4]
*v*C-N	1273 1174 1123 1084	1367 1248 1160	[9, 10]
*v*C-S	1006 952	1050 1031	[11]

νC-H rocking and out-of-plane bending	816 614	742 698 618	[12]

Table S4 Shows the comparative studies of the catalytic conversion of PATP to DMAB using multi metallic nanostructures.

Photo catalytic reaction	Photocatalyst	Conditions	Conclusions	Reference
PATP	Silver thin films evaporated on CaF_2 as silver substrate	0.1 mM solution of PATP adsorbed on silver substrate SERS and SERIA were recorded	Enhancement in peaks and some new peaks were originated called as b_2 modes	[13]
PATP	Au(core)/Cu(shell) nanoparticles	Au(core)/Cu(shell) nanoparticles were placed into an ethanolic solution of p-aminothiophenol (1.0mm), for 24 h, and then removed	b_2 and a_1 modes are all strong in intensity. Theoretical analysis was carried out to calculate electromagnetic and chemical enhancement.	[14]
PATP	silver-gold bimetallic hollow nanostructures	Silver-gold bimetallic structures deposited onto the silane modified glass soaked into $10^{-4}M$ *p*-ATP ethanol solution for around 2 h 514.5 nm and 1064 nm excitation.	Assigned new peaks as b_2 modes and calculated enhancement factor (EF)	[15]
PATP	Gold nanoparticles	p-ATP molecules were adsorbed on as-prepared substrates by spin-coating 5 µl of 1M solution on 2–2.5 cm^2	annealed gold nanoparticles for SERS experiments as well as a LSPR	[16]

		substrate area.	based sensor for biomolecule detection nanoparticle junctions as the important sites for Raman enhancement	
PATP	Ag NPs/PATP/Au NPs PATP molecules sandwiched between 85 nm sized Ag NPs and Au NPs with various shapes, including rods, tetrapods, spheres, cubes and dog-bones	ITO slides modified by a layer of Au NPs were immersed in 10^{-4} M PATP ethanol solutions for 12 h and immersed in Ag sols overnight	EM mechanism gives b_2 modes and EF was 10^8 b2 mode in SERS is characteristic of CT between the metal NPs and PATP molecules and may be likely greatly enhanced by CT from the Ag to Au NPs by tunneling through the PATP molecules.	[17]
PATP	Silver nanoplates on glass, gold and silver substrate	*p*-aminothiophenol (*p*-ATP) SAMs sandwiched in silver nanoplates and smooth macroscopic gold and silver substrates and SERS recorded at 514.5, 794.4, and 1064 nm excitations	strong electromagnetic coupling between the LSP of silver nanoplates and the SPP of the smooth macroscopic gold or silver EF values on the junctions are estimated to be as large as 10^4-10^5, which is 3-	[18]

			9 times larger than that on silver nanoplates deposited on glass	
PATP	Aggregates (size-200nm) of Au nanoparticle (13nm)	aggregation of AuNPs is induced by the addition of 2 mL of 2.6 μM p-aminothiophenol (p-ATP) to 2 mL of aqueous AuNP solution SERS – 785nm excitation	enhancement of the b2-symmetry bands occurs after 10 h enhancement of the b2 mode is attributed to the charge transfer (CT) between AuNPs and adsorbates,	[19]
PATP	PATP/Ag5 complex, PATP/Au5 complex, and Au5/PATP/Ag6 junction	514.4 and 632.8 nm	Theoretically predicted that selective enhancements of the b2 modes in SERS experiments should be due to the Herzberg–Teller mechanism via CT for metal/PATP complexes	[20]
PATP ➔ DMAB	Ag nanoparticles (40nm)	PATP- 5uM 632.8 nm	acquisition time is at 27 min for SERS measurement. The SERS enhancement is on the order of $\|M\|4=9.0 X10^8$ when illuminated the incident light of wavelength 632.8 nm. The total chemical enhancements,	[21]

			including static chemical and resonant enhancements, are on the order of 10^3.	
PATP ➔ DMAB	roughened Ag electrode.	potential dependent study of PATP on a roughened Ag electrode.	DMAB rather than PATP that gives the "*b*2 mode" signals laser used for the SERS excitation, can significantly induce the surface reaction of probed species.	[22]
PATP	AuNP-coated polymer substrate	PATP- 10^{-5} M	enormous b2-mode signal enhancement arose from the evaporationinduced reorientation of 4-aminobenzenethiol molecules adsorbed onto the AuNP surface	[23]
PATP ➔ DMAB	Ag nanoparticle-molecule-Ag (or Au) film.	Ag and Au films were immersed in a 5×10^{-6} M solution of PATP in ethanol for more than 5h	experimental and theoretical evidence that DMAB can be produced from PATP by surface nanoparticle-molecule- photochemistry reaction in the	[24]

			junctions of a Ag nanoparticle-molecule-Ag film DMAB cannot be produced from PATP in the junctions of a Ag nanoparticle-molecule-Au film. Electromagnetic enhancements 9 × 10^5 times in the junctions of Ag nanoparticle-PATP-Ag/Au films. chemical enhancement on the Au film – factor of 60	
PATP ➔ DMAB	Au, Ag, and Cu colloids	The solution of PATP in ethanol was introduced into capillary sample cells for normal Raman measurement. The solution of PATP in aqueous Au and Cu sols with 10^{-4}M concentrations was introduced into capillary sample cells for SERS measurement	In the neutral and alkaline conditions, PATP first can be easily deprotonated, then the deprotonated PATP is oxidized to DMAB. While in the acidic condition, PATP is hard to be oxidized, because of abundant Hþ in solution. When pH = 3, the surface	[25]

			photocatalysis reaction cannot occur; however under neutral and alkaline conditions (pH = 7 and 10), such a reaction does take place.	
PNTP ➔ DMAB	Au nanoplates And Ag tip	TERS (silver coated atomic force microscope tip to both enhance the Raman signal and to act as the catalyst) (532 nm) and red (633 nm)	first-of-a-kind study of a single catalytic 'particle' in action. TERS technique is unique in enabling the study of molecule dynamics and chemical reactions on a nanometre scale,	[26]
PNTP ➔DMAB PATP ➔ DMAB	Ag films in solutions with various pH values	514 and 633 nm lasers as exciting laser source to investigate the effect of photon's energy	theoretical and experimental investigation pH sensitivity of PATP reactions in acidic environment came from the amino group NH2.	[27]
PATP ➔DMAB➔PATP	single silver microsphere (1.5 mm in size)	completion in 5 min under N_2, no dimerization takes place	Dimerization of PATP into DMAB is actually induced	[28]

		whether O_2 or H_2O, must be involved in the plasmon-driven conversion of PATP into DMAB	by efficient energy transfer (plasmonic heating) from surface plasmon resonance to the surface adsorbed 4ATP, where O_2 (as an electron acceptor) is the necessary oxidant and H_2O (as a deprotonation agent) can enhance the reaction DMAB reduced to 4ATP, results from hot electron (from surface plasmon decay) induction at the metal surface to drive the reduction (bond scission) of the azo group, where H_2O or H_2 can act as a proton source.	
PNTP ➔DMAB	Single Ag particle with a diameter of 2 um	532nm exciation Reaction time 5 minutes	More enhancement is found under 532nm laser than that under 633nm higher power supplied for the 633 nm laser	[29]

			excitation can also dramatically accelerate the reaction	
PATP➔ DMAB Role of oxygen	Au film/PATP/Au NPs Ag film/PATP/Au NPs Au film/PATP/Ag NPs	activation of 3O2 by illumination of laser light and correlated it to the chemical properties of Au and Ag 532, 632.8, and 785 nm laser	yield of DMAB in the order of 632.8 nm> 785 nm>532 nm	[30]
PATP ➔ DMAB Role of hot electrons and holes	Ag nanoparticles	532nm laser	-Hole is revealed to be directly responsible for the oxidation of PATP to DMAB -role of O_2 is determined as an electron capturer to produce isolated holes.	[31]
PATP ➔ DMAB Activation of oxygen	Au@AgAu nanorattles, AgAu nanoshells and Au nanoparti cles	633nm laser	-hot electrons are transferred to adsorbed O_2 molecules	[32]
PNTP ➔DMAB Ultrafast Surface-Enhanced Raman Probing	Ag nanoparticles	518 nm pump pulse excitation source	-Hot electrons are responsible for reduction	[33]

PNTP ➔DMAB➔PATP	Bifunctional Au/Ag nanoparticle-decorated silicon nanowire arrays (Au/Ag@SiNWAs) ~~were~~	633nm laser	-excellent enhancement of the SERS signal, -real-time chemical reaction monitoring	[34]
PATP ➔ DMAB Photoactivated oxygen	spherical SiO_2 core densely decorated with Ag nanocubes (NCs),	785nm laser	-First order rate -Activated oxygen	[35]
PNTP ➔DMAB Hot electrons	Au and Au@SiO2	633 nm laser irradiation	-Au and pNTP have the highest utilization efficiency of hot electrons in the chemical bond state, more direct and efficient transfer mode. Compared with physical adsorption, the utilization efficiency of hot electrons in chemisorption was higher	[36]
PATP With and without oxygen, different products are formed	Au@TiO2 Au nanoparticles, Au@SiO2 nanoparticles and Au@SiO2@TiO	EC-SERS experiments were carried out with and without oxygen, on a range of nanostructures	“hot holes” induced by SPs can act as oxidizing agents in place of activated oxygen to oxidize the	[37]

	2		PATP and the nature of the interfaces plays a critical role. semiconductor as the charge transfer mediator is necessary for “hot holes” induced PATP oxidation, whose action can also improve hot electron induced oxygen activation.	
PATP ➔ DMAB Hot electrons	Au nanorods		oxygen that can be activated by the energetic plasmon electrons.	[38]
PATP ➔ DMAB -Different solvents -Holes are responsible for oxidation	Ag nanoparticles	-different diol solvents regulate the response of PATP to DMAB -solvent can quickly capture the hot electrons , so that the remaining holes can oxidize PATP to form DMAB. --The ability to trap hot electrons is different due to the difference in the position of the functional groups in the	-the activated oxidation pathway of oxygen does not play a leading role in this catalytic oxidation -hot electrons are rapidly captured by the solvent in the system for their	[39]

		solvent, so that the photocatalytic reaction rate of the hole-oxidized PATP is different	own hydroxyl reduction, leaving holes to oxidize the amino group of PATP	
PATP ➔ DMAB	multi-branched flowerlike gold (Au) nanostructures	785 nm excitation 10^{-5} M of PATP solution and Au nano Structure solution were mixed	strong electromagnetic field intensity around the sharp tips of the multibranched Au nanostructures	[40]
PNTP ➔ PATP Role of valence band states and plasmonic enhancemnet	Au nanoparticles	633 nm laser	pseudo-first-order kinetics	[41]

PATP- para aminothiophenol

PNTP- para nitrothiophenol

DMAB- p,p′-dimercaptoazobisbenzene

References

1. H. de Puig, J. O. Tam, C.-W. Yen, L. Gehrke and K. Hamad-Schifferli, *J. Phys. Chem. C*, 2015, **119**, 17408-17415.
2. K. Kalishwaralal, S. BarathManiKanth, S. R. K. Pandian, V. Deepak and S. Gurunathan, *Colloids Surf. B: Biointerfaces*, 2010, **79**, 340-344.
3. M. J. Oliveira, P. Quaresma, M. Peixoto de Almeida, A. Araújo, E. Pereira, E. Fortunato, R. Martins, R. Franco and H. Águas, *Sci. Rep*, 2017, **7**, 2480.
4. N. Karthik, S. Asha and M. Sethuraman, *J. Sol-Gel Sci. Technol.*, 2016, **78**, 248-257.
5. S.-H. Nam, T. K. Kim and J.-H. Boo, *Catal. Today*, 2012, **185**, 259-262.

6. F.-P. Du, N.-N. Cao, Y.-F. Zhang, P. Fu, Y.-G. Wu, Z.-D. Lin, R. Shi, A. Amini and C. Cheng, *Sci. Rep.*, 2018, **8**, 6441.
7. N. Masnabadi, M. H. Ghasemi, M. H. Beyki and M. Sadeghinia, *Res. Chem. Intermed.*, 2017, **43**, 1609-1618.
8. H. Li and Y. Li, *Nanoscale*, 2009, **1**, 128-132.
9. R. Biswas, H. Singh, B. Banerjee and K. K. Haldar, *ChemistrySelect*, 2019, **4**, 4003-4007.
10. R. Biswas, S. Mete, M. Mandal, B. Banerjee, H. Singh, I. Ahmed and K. K. Haldar, *J. Phys. Chem. C*, 2020, **124**, 3373-3388.
11. L.-N. Liu, J.-G. Dai, T.-J. Zhao, S.-Y. Guo, D.-S. Hou, P. Zhang, J. Shang, S. Wang and S. Han, *RSC adv.*, 2017, **7**, 35075-35085.
12. M. Ali, A. Mansha, S. Asim, M. Zahid, M. Usman and N. Ali, *J. Spectrosc.*, 2018, **2018**.
13. M. Osawa, N. Matsuda, K. Yoshii and I. Uchida, *J. Phys. Chem.*, 1994, **98**, 12702-12707.
14. L. Cao, P. Diao, L. Tong, T. Zhu and Z. Liu, *ChemPhysChem*, 2005, **6**, 913-918.
15. Y. Wang, H. Chen, S. Dong and E. Wang, *J. Chem. Phys*, 2006, **125**, 044710.
16. F. Toderas, M. Baia, L. Baia and S. Astilean, *Nanotechnology*, 2007, **18**, 255702.
17. X. Hu, T. Wang, L. Wang and S. Dong, *J. Phys. Chem. C*, 2007, **111**, 6962-6969.
18. Y. Wang, X. Zou, W. Ren, W. Wang and E. Wang, *J. Phys. Chem. C*, 2007, **111**, 3259-3265.
19. J. H. Yoon, J. S. Park and S. Yoon, *Langmuir*, 2009, **25**, 12475-12480.
20. M. Sun and H. Xu *ChemPhysChem*, 2009, **10**, 392-399.
21. Y. Fang, Y. Li, H. Xu and M. Sun, *Langmuir*, 2010, **26**, 7737-7746.
22. Y.-F. Huang, H.-P. Zhu, G.-K. Liu, D.-Y. Wu, B. Ren and Z.-Q. Tian, *J. Am. Chem. Soc*, 2010, **132**, 9244-9246.
23. N.-J. Kim, *J. Phys. Chem. C*, 2010, **114**, 13979-13984.
24. Y. Huang, Y. Fang, Z. Yang and M. Sun, *J. Phys. Chem. C*, 2010, **114**, 18263-18269.
25. M. Sun, Y. Huang, L. Xia, X. Chen and H. Xu, *J. Phys. Chem. C*, 2011, **115**, 9629-9636.
26. E. M. van Schrojenstein Lantman, T. Deckert-Gaudig, A. J. G. Mank, V. Deckert and B. M. Weckhuysen, *Nat. Nanotechnol*, 2012, **7**, 583-586.
27. Y. Huang and B. Dong, *Sci. China Chem.*, 2012, **55**, 2567-2572.

28. P. Xu, L. Kang, N. H. Mack, K. S. Schanze, X. Han and H.-L. Wang, *Sci. Rep*, 2013, **3**, 2997.
29. L. Kang, P. Xu, B. Zhang, H. Tsai, X. Han and H.-L. Wang, *Chem. Commun*, 2013, **49**, 3389-3391.
30. Y.-F. Huang, M. Zhang, L.-B. Zhao, J.-M. Feng, D.-Y. Wu, B. Ren and Z.-Q. Tian, *Angew. Chem*, 2014, **53**, 2353-2357.
31. X. Yan, L. Wang, X. Tan, B. Tian and J. Zhang, *Sci. Rep.*, 2016, **6**, 30193.
32. A. G. M. da Silva, T. S. Rodrigues, V. G. Correia, T. V. Alves, R. S. Alves, R. A. Ando, F. R. Ornellas, J. Wang, L. H. Andrade and P. H. C. Camargo, *Angew. Chem*, 2016, **55**, 7111-7115.
33. N. C. Brandt, E. L. Keller and R. R. Frontiera, *J. Phys. Chem. Lett*, 2016, **7**, 3179-3185.
34. P. Du, X. Zhang, H. Yin, Y. Zhao, L. Liu, Z. Wu and H. Xu, *Jpn. J. Appl. Phys*, 2018, **57**, 030308.
35. Q. Zhang and H. Wang, *J. Phys. Chem. C*, 2018, **122**, 5686-5697.
36. J. Chong, L. Wang, Y. Fu, K. Chen, R. Li and M. Huang, *Phys. E: Low-Dimens. Syst. Nanostructures*, 2020, **115**, 113699.
37. C. Zhan, Z.-Y. Wang, X.-G. Zhang, X.-J. Chen, Y.-F. Huang, S. Hu, J.-F. Li, D.-Y. Wu, M. Moskovits and Z.-Q. Tian, *J. Am. Chem. Soc*, 2019, **141**, 8053-8057.
38. T. E. Tesema, B. Kafle and T. G. Habteyes, *J. Phys. Chem. C*, 2019, **123**, 8469-8483.
39. Y. Liu, D. Yang, Y. Zhao, Y. Yang, S. Wu, J. Wang, L. Xia and P. Song, *Heliyon*, 2019, **5**, e01545.
40. M. He, B. Cao, X. Gao, B. Liu and J. Yang, *J. Mater. Res.*, 2019, **34**, 2928-2934.
41. R. Schürmann, K. Ebel, C. Nicolas, A. R. Milosavljević and I. Bald, *J. Phys. Chem. Lett*, 2019, **10**, 3153-3158.